Hindawi
International Journal of RF and Microwave Computer-Aided Engineering
Volume 2023, Article ID 9872407, 12 pages
https://doi.org/10.1155/2023/9872407

Research Article

A Wideband, Sharp Roll-Off U-Band Diplexer in Suspended Stripline Technology

Seyed-Milad Miri,[1] **Karim Mohammadpour-Aghdam**,[1] **and Seyed-Omidreza Miri**[2]

[1]*School of Electrical and Computer Engineering, University of Tehran, Tehran, Iran*
[2]*School of Electrical and Computer Engineering, Shiraz University, Shiraz, Iran*

Correspondence should be addressed to Karim Mohammadpour-Aghdam; kaghdam@ut.ac.ir

Received 14 January 2019; Accepted 30 July 2019; Published 17 May 2023

Academic Editor: Hai Wen Liu

This paper presents a low-loss, sharp roll-off, and wideband millimeter-wave contiguous diplexer implemented on 0.127 mm-thick TLY5 dielectric material to separate U-band frequency range into two jointed frequency ranges of 40-50 GHz and 50-60 GHz using two low-pass and high-pass filter channels. In order to integrate the diplexer in the front end of a wideband millimeter-wave down-converter and evaluate the frequency response, the proposed diplexer is supported by three add-on waveguide-to-suspended-stripline transitions. The final design of diplexer consisting of a low-pass filter with cut-off frequency of 50 GHz, a pseudo-high-pass filter with crossover at 50 GHz, and a T-junction is analyzed and optimized together with a 3D full-wave simulator. The realized diplexer features a VSWR of 2.5 : 1 across the entire operation frequency band of 40-60 GHz, low passband insertion loss of less than 2 dB in both channels, stopband rejection higher than 45 dB, and compact size with dimensions of $27 \times 13\ \text{mm}^2$ due to its intelligent and guided design and technology selection.

1. Introduction

Due to some attractive features of millimeter-wave frequency bands including channel safety, less spectral crowding, higher data rates, and increased spatial resolution, millimeter-wave devices have been used in various applications such as transceivers, automotive radars, and imaging systems [1–3]. Diplexers, either planar or nonplanar configurations, are usually used in the front end of modern communication systems and test instruments where broadband common input signal has to be separated into two distinct subbands for further signal processing. Also, diplexers can be used to transmit and receive signals by applying a single antenna. Furthermore, diplexers can reduce the number of RF-components which are needed for subchannels in single receiving mode. So to meet these requirements, contiguous diplexers with low insertion loss, high isolation between subchannels, sharp band-edge roll-off, and high selectivity are needed. Diplexers are usually made of low-pass and high-pass filters or they are designed by a combination of bandpass filters. These filters can be connected to each other by different structures such as E-plane and H-plane power dividers, circulators, Y-junctions, and T-junctions which may be the most popularly used combining circuits [4–7].

Although microstrip planar diplexers have been extensively studied in recent years because of advantages, such as compact size, easy fabrication, and integration capability [8, 9], they suffer from high losses and low power transmission capability. However, waveguide diplexers have low loss and high isolation between channels, but they are massive and relatively expensive; consequently, they are not suitable for integrated circuits [10, 11]. The suspended stripline (SSL), which has a substrate suspended symmetrically between two ground planes, has some attractive features including lower loss over wider frequency range of operation, flat group delay, and better temperature stability compared with microstrip and stripline [12]. Thickness of dielectric layer is much smaller than cavity height resulting in an effective dielectric constant near to one. Hence, quasi-TEM will be a dominant propagation mode causing wider frequency range of operation with less dispersion and lower dielectric loss. Also, SSL has lower current density

on the metal leading to lower conduction loss and higher Q factor. Besides, small changes in dielectric constant due to temperature variations have small impact on the propagation characteristics. Therefore, SSL has better temperature stability. Furthermore, the shielding metal enclosure blocks the radiation from other parts of the system.

In recent years, various multiplexers with very good functionality have been presented, while most of them are usually narrowband, noncontiguous, or have both disadvantages [13–15]. However, some contiguous and wideband multiplexers also have been proposed. In Ref. [16], a contiguous planar diplexer in SSL technology with two channels from DC to 40 GHz and 40 to 80 GHz has been presented. This diplexer features rejection of around 30 dB at 40% away from crossover. Ashiq and Khanna have proposed some ultrabroadband contiguous diplexers using SSL technology with a combination of low loss and steep band-edge low-pass and high-pass channels [17–19]. Ref. [17] describes a planar diplexer with stopband rejection of around 38 dB in both channels, including DC-35 GHz and 35-65 GHz, while its 30 dB roll-off point is at 10% away from crossover. Also, Ref. [18] presents a hybrid nonplanar diplexer covering DC-36 GHz and 36-66 GHz channels. This diplexer, implemented using waveguide and SSL technologies, has stopband rejection of around 30 dB with 30 dB roll-off point at 7.6% away from crossover. They also proposed another planar diplexer using liquid crystal polymer (LCP) in Ref. [19]. The low-pass and high-pass channels of this design cover bandwidth of DC-66 GHz and 66-100 GHz with stopband rejection of 35 dB, and insertion loss falls below 30 dB at 7.5% away from crossover. However, high precision fabrication process is required to implement this design.

This paper presents a wideband and contiguous diplexer to be used in the front end of an integrated U-band down-converter as shown in Figure 1. In this down converter, the received signal by a U-band pyramidal horn antenna is guided by WR19 standard waveguide, and then, the 40-60 GHz input signal is delivered to an integrated board through a WR19 waveguide-to-SSL transition.

This diplexer separates the incoming amplified output signal of a low noise amplifier (LNA) into two jointed frequency bands of 40-50 GHz and 50-60 GHz. Then, these high frequency subbands are down-converted to frequency range of 5-15 GHz which is suitable for further signal processing.

Figure 2 demonstrates a contiguous diplexer combining shunt low-pass and high-pass filters connected with a common junction. To minimize reflections and obtain matched input, the complex input admittances, Y_{LPF} and Y_{HPF}, of two filters should satisfy the equation below at all frequencies [16]:

$$Y_{\mathrm{in}} = Y_{\mathrm{LPF}} + Y_{\mathrm{HPF}} = Y_0. \tag{1}$$

Considering purely real reference admittance Y_0, the above condition can be separated into two following conditions [16]:

$$\begin{aligned} \mathrm{Re}\,(Y_{\mathrm{LPF}}) + \mathrm{Re}\,(Y_{\mathrm{HPF}}) &= Y_0, \\ \mathrm{Im}\,(Y_{\mathrm{LPF}}) + \mathrm{Im}\,(Y_{\mathrm{HPF}}) &= 0. \end{aligned} \tag{2}$$

The diplexer comprised two low-pass and pseudo-high-pass filter channels connected to WR19 waveguide-to-SSL transitions. The low-pass and pseudo-high-pass filters are realized using the 13^{th}-order generalized Chebyshev and 13^{th}-order Chebyshev low-pass prototypes, respectively, in SSL technology to achieve low loss and wideband filters with sharper band-edge roll-off response and better stopband rejection over wider bandwidth. The diplexer is implemented on a 0.127 mm-thick TLY5 substrate with a dielectric constant of 2.2 and loss tangent of 0.009 which is suspended symmetrically in a metal waveguide channel with maximum width of 2 mm and 0.961 mm height. To complete the construction of diplexer, two filters are connected to each other by an input common T-junction, and then, the first series and the first shunt elements of both of them are optimized to have good impedance matching. Following this, WR19 waveguide-to-SSL transitions are added to filter ports to be able to integrate the proposed diplexer in the front end of a millimeter-wave U-band down-converter. Full-wave simulation is further used to validate the diplexer design. Then, experiment is conducted to verify the diplexer performance.

2. Design and Simulation

Herein, a wideband contiguous diplexer is needed to be used in the front end of a U-band down-converter with design specifications described in Table 1.

The structure of diplexer is comprised of a low-pass filter connecting to a pseudo-high-pass filter in parallel with a common input T-junction. To form a contiguous diplexer, filters should satisfy equation (1) which are usually known as complementary filters. Design of filters must be started with an appropriate low-pass prototype to satisfy the aforementioned design specifications.

A lumped-element contiguous diplexer can be considered as a network realized by shunting low-pass and high-pass sections as shown in Figure 3 in which N indicates the degree of filters. As mentioned, low-pass channel is realized by the generalized Chebyshev prototype. Each shunt resonant branch of the distributed generalized Chebyshev low-pass prototype can be represented by a capacitive branch and hence shunt open circuit stub. So lumped-element circuit can be shown as Figure 3 in which the values of the first series and the first shunt normalized elements of each channel are illustrated. To achieve good impedance matching in contiguous diplexer, the first series and the first shunt elements of low-pass and high-pass sections must be modified. So to form a diplexer with desirable specifications, two filters must be designed individually in the first step. Then, they should be connected to each other by means of a wideband common input junction. The final step involves optimizing the first elements of both filters to obtain well-matched input port.

As discussed, different technologies can be applied to realize a diplexer. Herein, max-to-min characteristic impedance ratio and nominal insertion loss versus frequency of a suspended stripline and a microstrip line are compared and shown in Figure 4. As seen, insertion loss in both cases increases at higher frequencies, while microstrip has much more losses compared to SSL. Also, max-to-min achievable

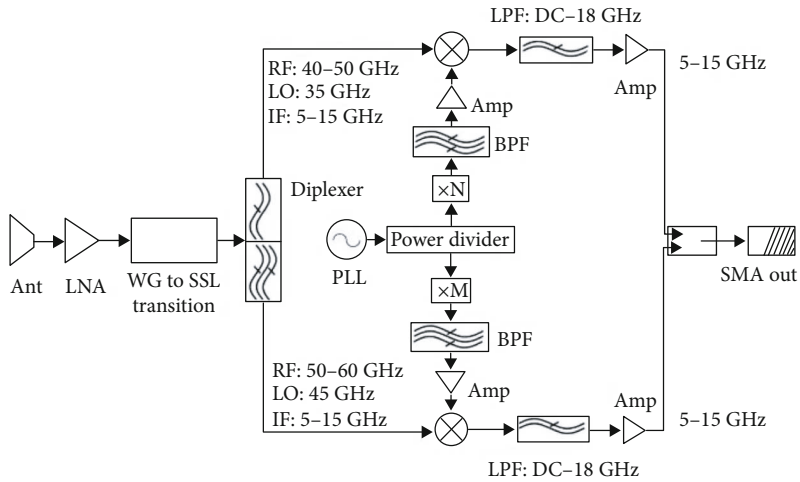

Figure 1: U-band down-converter block diagram.

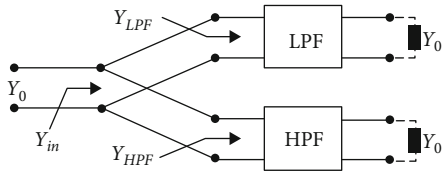

Figure 2: Schematic of contiguous diplexer.

Table 1: Design Specifications.

Parameter	Value	Freq. range
Input VSWR	2.5 : 1	40–60 GHz
Passband loss	≤2 dB	40–60 GHz
Crossover insertion loss	≤7 dB	At 50 GHz
Stopband rejection	≥45 dB	10% away from cut-off

characteristic impedance ratio of two transmission lines is compared as demonstrated in Figure 4. As seen, although the realizable impedance ratio in SSL technology is 20% smaller than microstrip technology, SLL enjoys extremely low insertion loss, which is one fifth of the microstrip technology (0.05 dB/cm in comparison with 0.25 dB/cm of microstrip technology). Nevertheless, distributed circuit of diplexer is realized using SSL technology due to its advantages. The low-pass filter is implemented on one side of the substrate, while pseudo-high-pass filter is realized on both sides of the substrate to achieve tight coupling by forming broadside-coupled sections.

Higher-order mode propagation and unwanted resonances within the cavity are important concerns which must be considered in design of millimeter-wave suspended stripline devices because they can destroy the attenuation or rejection characteristics of filters. For proper single mode operation up to desirable frequency, dimensions of SSL cross-section must be determined in the first step. To ensure that dominant propagation mode is quasi-TEM in operation frequency band, the cut-off frequency of SSL is set to be above 75 GHz. The cut-off frequency is calculated from the equation below [20]:

$$f_c = \frac{c}{2a}\sqrt{1 - \frac{h}{b}\left(\frac{\varepsilon_r - 1}{\varepsilon_r}\right)}, \tag{3}$$

where a and b are the width and the height of channel, respectively, c is the speed of light, h is the substrate height, and ε_r is the relative permittivity of the substrate.

Figure 5 indicates how the width of cavity affects the cut-off frequency of TE_{10} mode in terminal ports of SSL structure. As shown in Figure 5, reducing the cavity width moves the cut-off frequency of TE_{10} mode to higher frequencies. Thus, for single mode operation up to 75 GHz, the width of waveguide channel has to be smaller than 2 mm.

Also, to ensure that no unwanted resonance happens along the height of cavity in desirable frequency band of operation, b is set to be smaller than $\lambda/4$ at 75 GHz.

2.1. Low-Pass Filter Design. To design low-pass filter with cut-off frequency of 50 GHz with passband ripple of 0.1 dB and specifications mentioned in Table 1, a 13^{th}-order generalized Chebyshev low-pass prototype is considered. A generalized Chebyshev prototype is more preferred rather than the conventional Chebyshev because it can achieve high selectivity according to design specification due to transmission zeros at order $(N-1)$ at a finite frequency near to band-edge and a single zero at infinity. However, elliptic function prototype is realized with minimum possible degree for a given selectivity and passband ripple, but physical realization of the generalized Chebyshev prototype with the same degree and close selectivity is much easier due to smaller range of impedance variations which are required to realize a printed circuit [21].

Authors recently published a paper [12] and completely described the design method of single low-pass filter using the 13^{th}-order generalized Chebyshev prototype in SSL technology. Also, simulation and measurement results of single low-pass filter have been presented in Ref. [12].

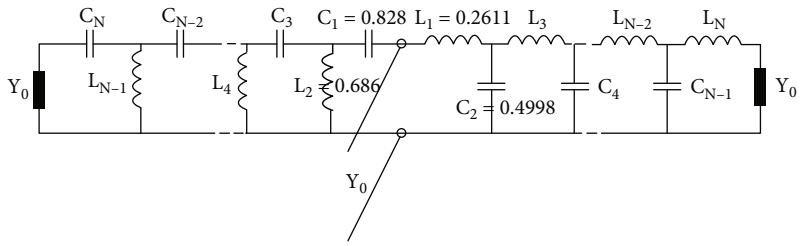

Figure 3: Lumped-element prototype of contiguous diplexer.

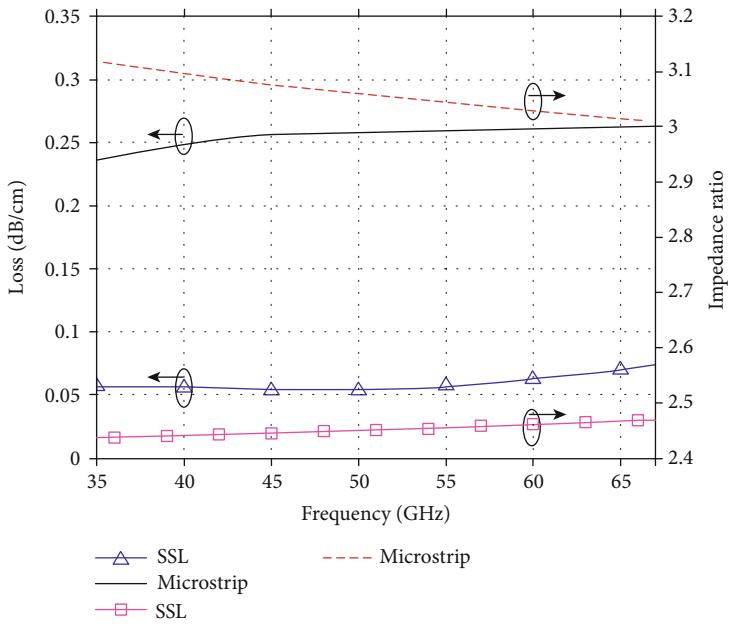

Figure 4: Comparison of the insertion loss and the max-to-min characteristic impedance ratio of microstrip line and SSL with cavity height of 0.961 mm and cavity width of 1.5 mm.

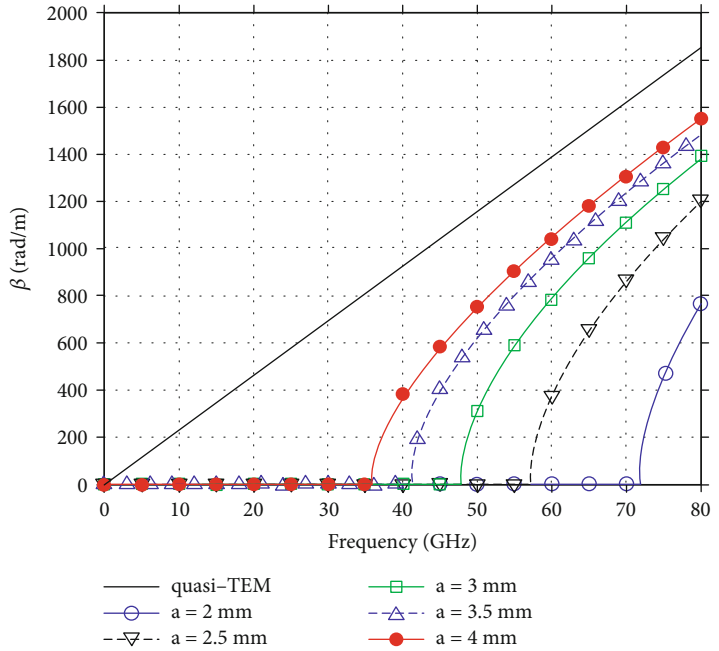

Figure 5: Cut-off frequency of higher-order modes versus channel width (a).

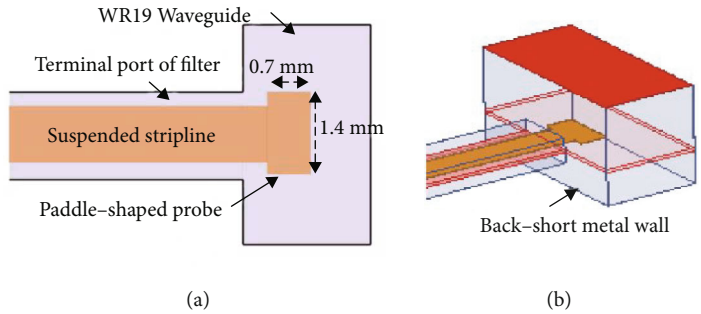

FIGURE 6: WR19 waveguide-to-SSL transition: (a) top view, (b) 3D view.

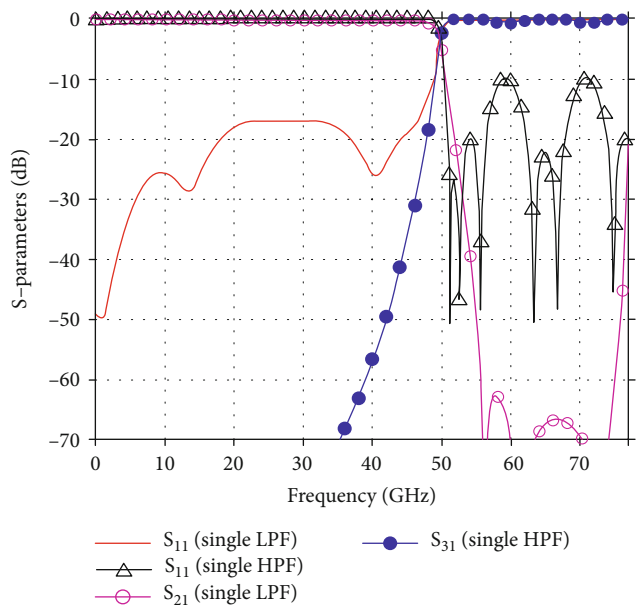

FIGURE 7: S-parameter simulation results of single low-pass and single pseudo-high-pass filters.

2.2. Pseudo-High-Pass Filter Design. Many filtering circuits are designed based on coupled transmission lines. To realize ultrawideband filters, tightly coupled resonators with very small separation distance are required. So design and realization of millimeter-wave circuits using capacitive gap-coupled transmission lines and paralleled-coupled resonators are too difficult due to the critical tolerance of fabrication. SSL technology can be used to overcome the limits of line separation, and hence, much larger range of required impedance values can be realized using broadside-coupled lines. Broadside-coupled suspended stripline, firstly analyzed by Bhartia and Pramanick [22], benefits from tight coupling and low loss making it suitable for designing microwave and millimeter-wave devices. In this contribution, a broadband filter is designed using coupled line SSL resonators on both sides of the substrate. Indeed, this filter is a bandpass filter with wide enough passband which functions as a pseudo-high-pass filter in the operation frequency band.

Here, the 13^{th}-order Chebyshev low-pass prototype is used to design a broadband pseudo-high-pass filter with cut-off frequency of 50 GHz, passband ripple of 0.1 dB, and specifications given in Table 1. This filter is realized using edge-coupled $\lambda/2$ resonators in which the overlapping length of broadside-coupled sections determines values of the series capacitances. Based on the design approach of coupled line filters established in Ref. [23] and by given normalized element values of the Chebyshev prototype, the corresponding even- and odd-mode impedances and relevant effective dielectric constants of coupled line sections are determined [24]. The length of each resonator is ideally half wavelength at the center frequency of passband, but because of different values for even- and odd-mode effective dielectric constants, the exact length of resonators can be determined as equations developed in Ref. [25]. By setting the internal impedance levels to have resonators with desired Q factor, the width of coupled lines is calculated using the equations in Ref. [12] with respect to channel dimensions.

2.3. Waveguide-to-Suspended-Stripline Transition. To measure the response of diplexer up to millimeter-wave frequencies, three WR19 waveguide-to-SSL transitions are necessary to be integrated with diplexer ports. These transitions should be able to guide maximum energy from TE_{10} dominant mode of WR19 standard U-band waveguide to quasi-TEM

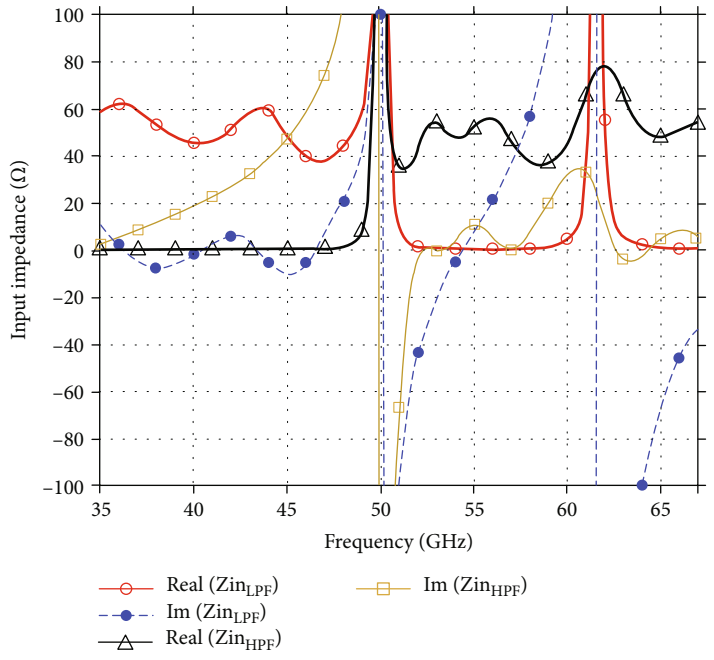

(a)

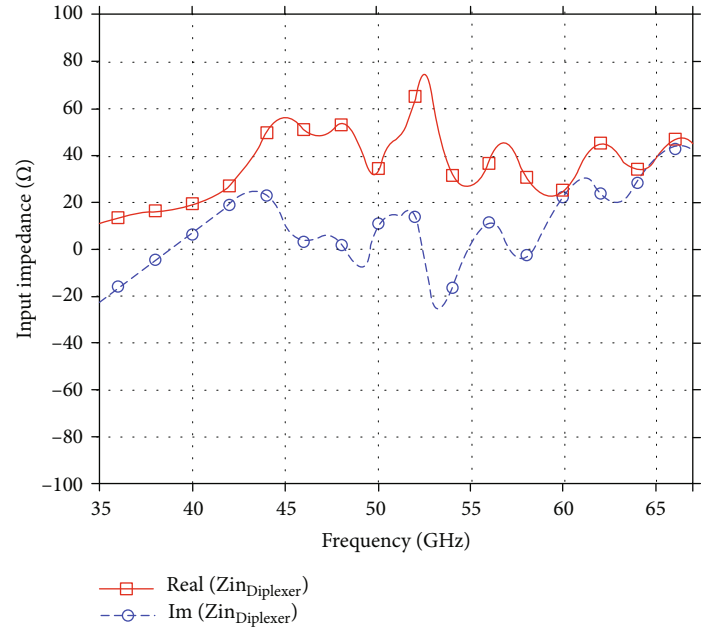

(b)

FIGURE 8: (a) Input impedance of single low-pass and single pseudo-high-pass filters. (b) Input impedance of diplexer formed by shunting low-pass and pseudo-high-pass filters.

mode in SSL. Herein, a broadside probe-type transition, demonstrated in Figure 6, is used. The probe is an extension of suspended stripline into the waveguide so that its surface faces the direction of propagation in the waveguide. Probe shape and inserted stub into the waveguide are critical parameters to achieve good matching and mode conversion. Also, the distance between the probe and the back-short metal wall is determined equal to one quarter of guided wavelength, $\lambda_g/4$, to flow maximum energy in propagation direction.

2.4. Simulation. Designed structures including low-pass filter, pseudo-high-pass filter, and WR19 waveguide-to-SSL transition are analyzed using a 3D full-wave simulator.

Dimensions of low-pass filter are optimized so that design specifications are satisfied. The filter comprises of shunt stubs with different lengths and hence different resonance frequencies leading to wider stopband. Stepped impedance resonators also result in better impedance matching with common transmission line. The simulated S-parameters of low-pass filter after final optimizations are

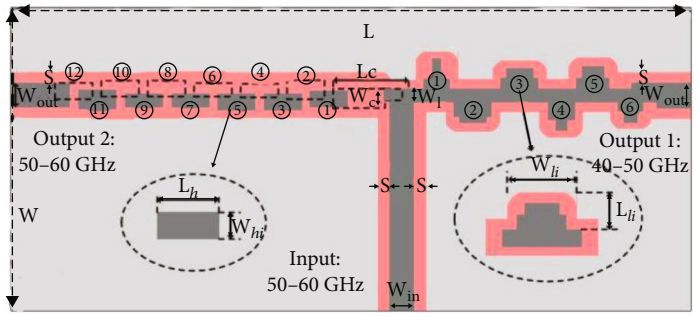

Figure 9: 2D layout of diplexer.

Table 2: Dimensions of diplexer.

Parameter	Value (mm)	Parameter	Value (mm)	Parameter	Value (mm)
$W_{h1} = W_{h12}$	0.6	W_{l1}	1.55	L_{l1}	1.4
$W_{h2} = W_{h11}$	0.7	W_{l2}	2	L_{l2}	1.1
$W_{h3} = W_{h10}$	0.6	W_{l3}	2	L_{l3}	1.06
$W_{h4} = W_{h9}$	0.5	W_{l4}	1.6	L_{l4}	1.36
$W_{h5} = W_{h8}$	0.6	$\boldsymbol{W_{l5}}$	1.8	$\boldsymbol{L_{l5}}$	1.15
$W_{h6} = W_{h7}$	0.5	W_{l6}	1.5	L_{l6}	1.03
W_{in}	0.9	W_l	0.5	L_h	1.4
W_{out}	0.9	W_c	0.8	L_c	2.8
S	0.3	W	13	L	27

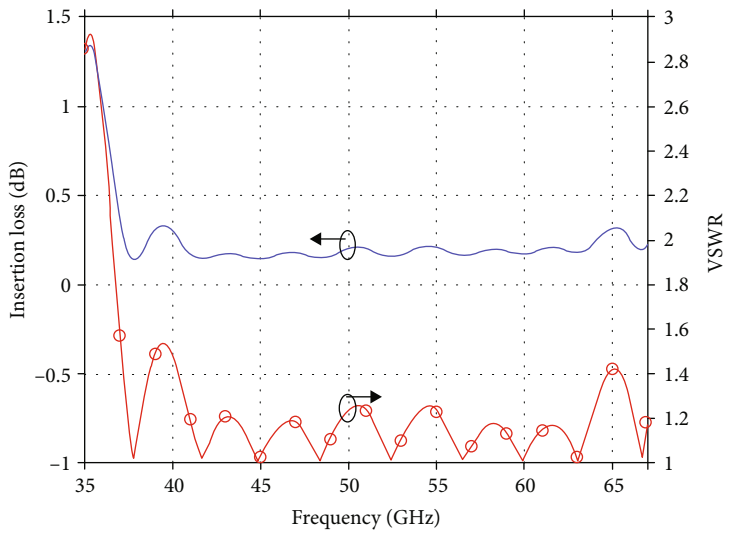

Figure 10: VSWR and insertion loss of back-to-back WR19 waveguide-to-SSL transition.

illustrated in Figure 7. The return loss is better than 10 dB in DC-50 GHz with very low passband insertion loss. Designed filter also shows high selectivity and wideband rejection of higher than 45 dB except within 9.2% of band-edge frequency.

The configuration of pseudo-high-pass filter includes SSL resonators with different strip widths and offsets. These parameters are optimized such that good impedance matching and resonators with desired Q factor are obtained. S-parameters of simulated pseudo-high-pass filter are demonstrated in Figure 7. The filter response shows the return loss better than 10 dB in 50-75 GHz with very low insertion loss due to SSL. This filter has almost sharp rejection so that S_{31} falls 45 dB at 13.8% away from the band-edge.

After the design of low-pass and high-pass filters, it is time to form diplexer by shunting two filters through an input common T-junction. Figure 8 demonstrates input impedance of single low-pass and single pseudo-high-pass filters as well as input impedance of diplexer after

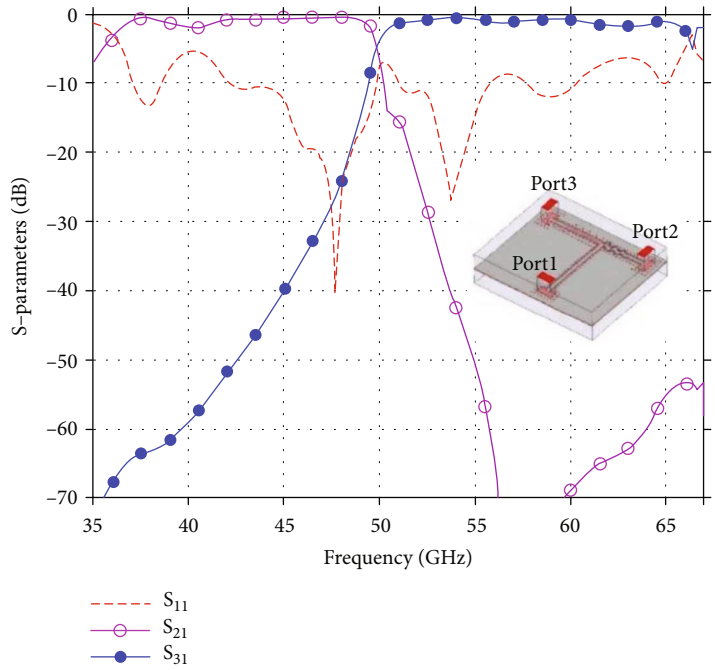

Figure 11: S-parameter simulation result of designed diplexer. Inset picture shows 3D view of designed diplexer.

connecting filters with common input junction. As seen in Figure 8(a), both filters have suitable input impedance in their passband, while they affect each other when they are connected as shown in Figure 8(b). By connecting filters, the first series and the first shunt elements of two filters may resonate with each other causing undesirable notch in the passband of diplexer channels. So the length and the width of first capacitive and inductive sections of both low-pass and high-pass channels must be optimized to have good VSWR across the entire bandwidth of diplexer. The 2D layout of diplexer consisting of low-pass filter, pseudo-high-pass filter, and common T-junction is demonstrated in Figure 9. The diplexer dimensions, shown in Figure 9, are listed in Table 2. The low-pass filter is implemented on the single side of the substrate while the strips determined by dash lines show coupled sections of pseudo-high-pass filter on the opposite side of the substrate.

Based on the described approach, an optimal transition, as illustrated in Figure 6, is designed using TLY5 substrate with a thickness of 0.127 mm and then analyzed by a full-wave simulator. Input VSWR and insertion loss of designed back-to-back transition are presented in Figure 10. As seen, input VSWR is better than 1.5 : 1 over the entire 37-67 GHz, and insertion loss is lower than 0.5 dB.

To complete the structure of diplexer, WR19 waveguide-to-SSL transitions are added to terminal ports of filter channels as shown as an inset picture in Figure 11. Since three U-band coaxial-to-waveguide adaptors are required to evaluate the diplexer performance and also to ensure that waveguide modes will not be propagating in the desirable operation frequency band, the input and output transmission line sections of filters are extended with respect to the adaptor dimensions. However, high rejection of designed filters also suppresses higher-order waveguide modes at terminal ports of structure. Simulation results of the entire diplexer including transitions can be found in Figure 11. As seen, input VSWR is better than 2.5 : 1(a return loss of better than 7.3 dB) over the entire 40-60 GHz except around 40 GHz where it increases to 3.3 : 1. To find the reason, current distribution on diplexer at 40 GHz is computed and depicted in Figure 12(a). As illustrated in Figure 12(b), the resonance of first series and first shunt elements of filters occurring at 31.2 GHz affects the VSWR at 40 GHz. For better results, this resonance frequency should be moved away to lower frequency. But the cut-off frequency of dominant TE_{10} mode limits this improvement. The passband insertion loss of both channels is lower than 2 dB. Also both channels have wide-band rejection of higher than 45 dB and sharp rejection such that the insertion loss of low-pass and high-pass channels falls below 45 dB at 8.7% and 12.3% away from the crossover, respectively. The crossover point is at 49.9 GHz with insertion loss of 5 dB.

3. Fabrication and Measurement

The box of the structure is made using brass. The box consists of two parts so that printed circuit board (PCB) is located between them, and they are fastened to each other with prepared screws. Two parts of the metal box is electrically connected by the rows of vias along the edges of the waveguide channels. Also, some alignment pins provide accurate positioning of the suspended stripline in waveguide cavity. The transitions are also implemented as a part of the whole box.

Figure 13 demonstrates the fabricated diplexer. For S-parameter measurement, U-band 1.85 mm coaxial-to-waveguide adaptors are added to the diplexer structure. An Agilent vector network analyzer (VNA) is used for

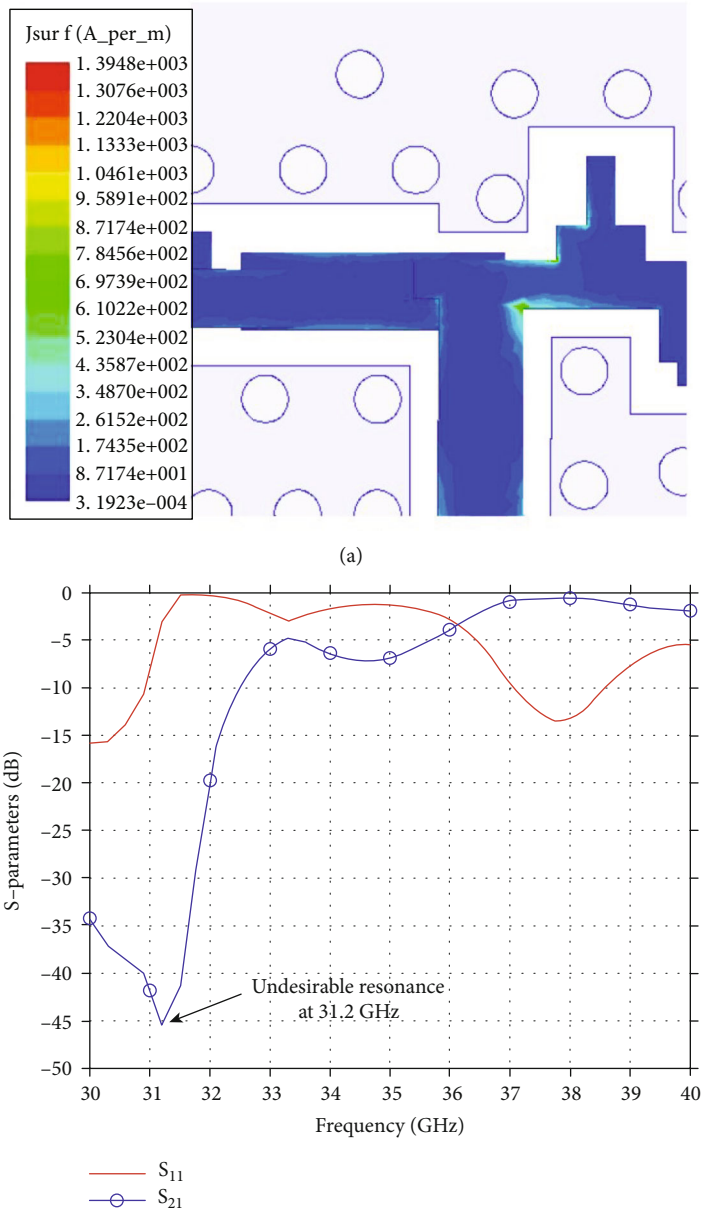

Figure 12: (a) Current distribution on first element of both filters connected by common input T-junction at 40 GHz. (b) S-parameter simulation result of designed diplexer in frequency band of 30-40 GHz showing undesirable resonance at 31.2 GHz.

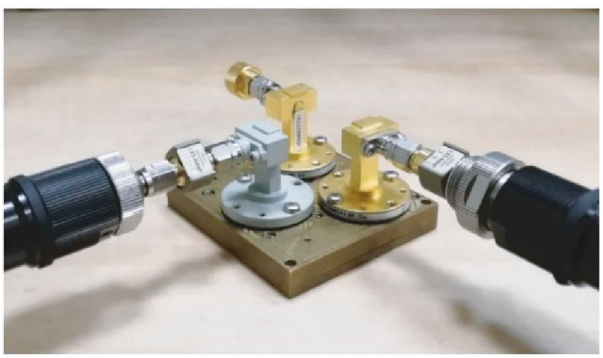

Figure 13: Fabricated diplexer connected to VNA ports and matched to 50 Ohm load at one port.

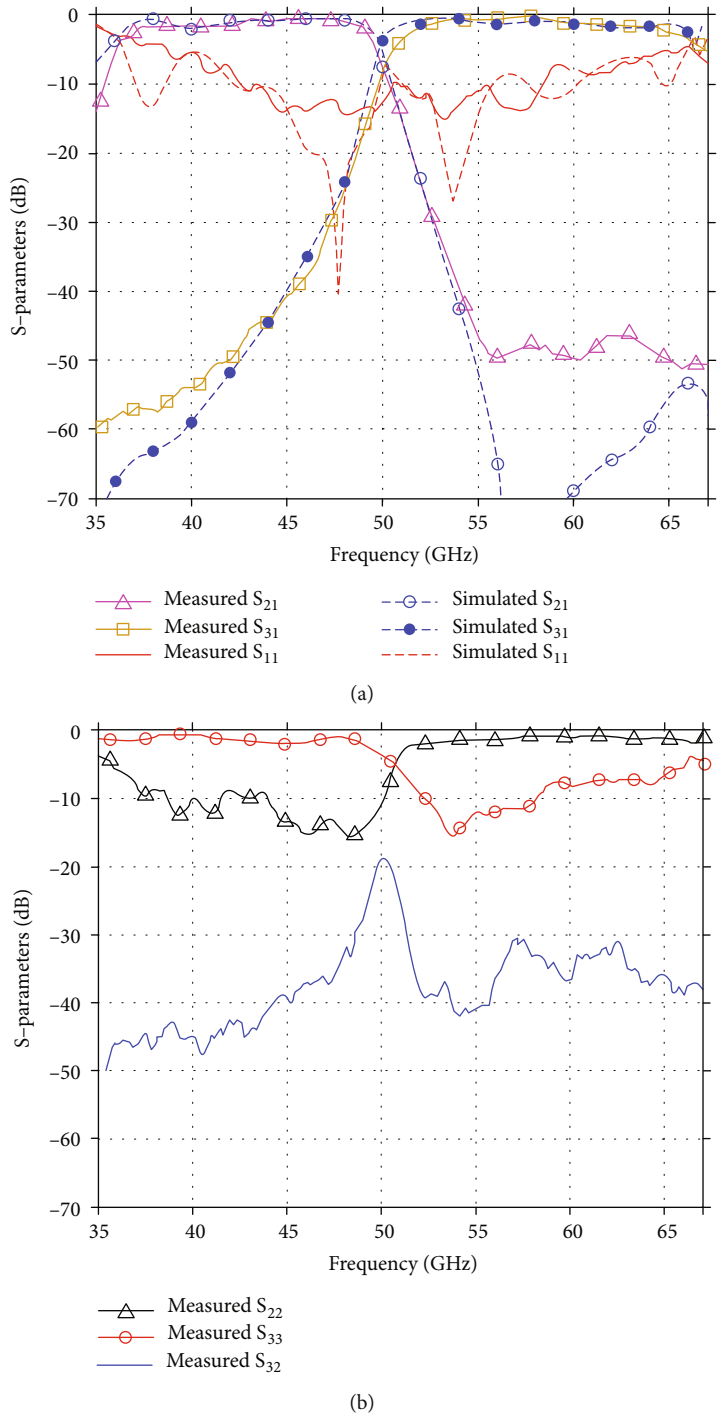

Figure 14: Measured S-parameters of fabricated diplexer: (a) input return loss and insertion loss of both channels, (b) isolation and return loss of output ports.

measuring the diplexer response. As network analyzer provides only two ports, during measurement of each filter channel's response, the other output port is matched to 50 Ohm load. Before measuring the S-parameters of the diplexer structure, the through connection was formed by connecting two adaptors directly back to back. By measuring the S-parameters of this back-to-back configuration, the filter response from output of adaptors as reference planes can be determined.

Figure 14(a) shows measured S-parameters from defined reference planes as well as simulation results of the realized diplexer. Both simulation and measurement results include WR19 waveguide-to-SSL transitions. Measured results display a return loss of better than 7.3 dB (VSWR <2.5 : 1) and a maximum insertion loss of 2 dB at operation frequency band of 40-60 GHz. However, the return loss approaches to 5.5 dB near 40 GHz in agreement with simulation results. Both filters show high rejection and sharp roll-

Table 3: Comparison between diplexers in this article and other works.

References	Substrate	Substrate thickness (mm)	Maximum insertion loss (dB)	30 dB roll-off point	Stopband rejection (dB)
[16]	Alumina	0.127	1.8	40%	30
[17]	RT/duroid5880	0.127	1.3	10%	38
[18]	RT/duroid5880	0.127	1.5	7.6%	30
[19]	LCP	0.0508	5	7.5%	35
This work	TLY5	0.127	2	6%	45

off so that both low-pass and high-pass channels have a wideband rejection of higher than 45 dB except almost 9.4% and 13.3% of band-edge frequency, respectively. The crossover is measured at 50.1 GHz with insertion loss of 7 dB. Figure 14(b) also displays the measured isolation and return loss of output ports. The proposed diplexer has a good isolation of higher than 30 dB between two outputs except almost 2.8% away from crossover. Also, output VSWR is better than 2.5 : 1 (a return loss of better than 7.3 dB) over the entire 40-60 GHz frequency range. So the measured results are relatively in good agreement with the simulation response of diplexer if considering the complexity of the circuit and fabrication tolerance. Therefore, the small shift in frequency of crossover and the observed deviations between simulation and measurement results are probably caused by manufacturing tolerances and marginal excitation of higher-order modes. In Table 3, the achieved results for proposed diplexer are compared with respect to earlier works in Refs. [16–19]. All these works have been implemented using the conventional Chebyshev low-pass prototype while our design enjoys the 13^{th}-order generalized Chebyshev as low-pass channel and the 13^{th}-order Chebyshev as high-pass channel. Indeed, the proposed design has better selectivity and higher stopband rejection in wide bandwidth of 40-60 GHz rather than the earlier works as compared in Table 3. The realized diplexer also benefits from compact size so that by excluding feeding lines and transitions, its dimensions are only $27 \times 13\,\text{mm}^2$.

4. Conclusion

A wideband contiguous diplexer in suspended stripline technology with low-pass and high-pass channels covering 40-50 GHz and 50-60 GHz, respectively, is implemented on a TLY5 dielectric material with a dielectric constant of 2.2. Three WR19 standard waveguide-to-SSL transitions with VSWR of better than 1.5 : 1 across the entire 37-67 GHz have been added to diplexer ports allowing integration in the front end of a U-band millimeter-wave down-converter and evaluation of diplexer response. The diplexer has a VSWR better than 2.5 : 1 across the almost frequency range of 40-60 GHz with low insertion loss of less than 2 dB. Also, the diplexer features high stopband rejection of better than 45 dB with sharp rejection so that 45 dB roll-off point for low-pass and high-pass channels is at 9.4% and 13.3% away from the crossover at 50.1 GHz, respectively. Furthermore, the proposed diplexer has a good isolation of higher than 30 dB between two outputs except almost 2.8% away from crossover. However, small observed deviations between simulation and measurement results are mainly caused by fabrication errors such as the tolerance on low-cost etching of PCB, box milling error, inaccurate alignment of suspended striplines in waveguide channels, marginal excitation of higher-order modes, and effects of undesirable resonance frequencies.

Data Availability

All data supporting the study are included in this article. The materials and data in the current study are available from the authors upon reasonable request.

Conflicts of Interest

The authors declare no potential conflicts of interest.

Acknowledgments

The authors would like to acknowledge ZAEIM Electronic Industries for partial support of this work.

References

[1] K. Ohata, K. Maruhashi, M. Ito, and T. Nishiumi, "Millimeter-wave broadband transcievers," *NEC Journal of Advanced Technology*, vol. 2, no. 3, pp. 211–216, 2005.

[2] J. Hasch, E. Topak, R. Schnabel, T. Zwick, R. Weigel, and C. Waldschmidt, "Millimeter-wave technology for automotive radar sensors in the 77 GHz frequency band," *IEEE Transactions on Microwave Theory and Techniques*, vol. 60, no. 3, pp. 845–860, 2012.

[3] L. Yujiri, M. Shoucri, and P. Moffa, "Passive millimeter wave imaging," *IEEE Microwave Magazine*, vol. 4, no. 3, pp. 39–50, 2003.

[4] J. A. Ruiz-Cruz, J. R. Montejo-Garai, J. M. Rebollar Machain, and S. Sobrino, "Compact full Ku-band triplexer with improved E-plane power divider," *Progress In Electromagnetics Research*, vol. 86, pp. 39–51, 2008.

[5] C. E. Saavedra, "Diplexer using a circulator and interchangeable filters," in *2008 7th International Caribbean Conference on Devices, Circuits and Systems*, pp. 1–5, Cancun, Mexico, 2008.

[6] S. Bastioli, L. Marcaccioli, and R. Sorrentino, "An original resonant Y-junction for compact waveguide diplexers," in *2009 IEEE MTT-S International Microwave Symposium Digest*, pp. 1233–1236, Boston, MA, USA, 2009.

[7] T. V. Duong, W. Hong, Z. C. Hao, W. C. Huang, J. X. Zhuang, and V. P. Vo, "A millimeter wave high-isolation diplexer using selectivity-improved dual-mode filters," *IEEE Microwave and Wireless Components Letters*, vol. 26, no. 2, pp. 104–106, 2016.

[8] C. F. Chen, T. Y. Huang, C. P. Chou, and R. B. Wu, "Microstrip diplexers design with common resonator sections for compact size, but high isolation," *IEEE Transactions on Microwave Theory and Techniques*, vol. 54, no. 5, pp. 1945–1952, 2006.

[9] G. Moloudian and M. Dousti, "Design and fabrication of a compact microstrip lowpass-bandpass diplexer with high isolation for telecommunication applications," *International Journal of RF and Microwave Computer-Aided Engineering*, vol. 28, no. 5, article e21248, 2018.

[10] L. Zhu, R. R. Mansour, and M. Yu, "Compact waveguide dual-band filters and diplexers," *IEEE Transactions on Microwave Theory and Techniques*, vol. 65, no. 5, pp. 1525–1533, 2017.

[11] F. M. Vanin, D. Schmitt, and R. Levy, "Dimensional synthesis for wide-band waveguide filters and diplexers," *IEEE Transactions on Microwave Theory and Techniques*, vol. 52, no. 11, pp. 2488–2495, 2004.

[12] S. M. Miri, K. Mohammadpour-Aghdam, and S. O. Miri, "A millimeter-wave high selective lowpass filter in suspended stripline technology," in *2018 Fifth International Conference on Millimeter-Wave and Terahertz Technologies (MMWaTT)*, pp. 12–15, Tehran, Iran, 2018.

[13] C. Arnold, J. Parlebas, R. Meiser, and T. Zwick, "Fully reconfigurable manifold multiplexer," *IEEE Transactions on Microwave Theory and Techniques*, vol. 65, no. 10, pp. 3885–3891, 2017.

[14] H. Sajadinia, M. Dahmardeh, and M. Khalaj-Amirhosseini, "Novel planar diplexer using branch-line coupler," *Microwave and Optical Technology Letters*, vol. 60, no. 11, pp. 2773–2777, 2018.

[15] S. Srisathit, S. Patisang, R. Phromloungsri, S. Bunnjaweht, S. Kosulvit, and M. Chongcheawchamnan, "High isolation and compact size microstrip hairpin diplexer," *IEEE Microwave and Wireless Components Letters*, vol. 15, no. 2, pp. 101–103, 2005.

[16] R. Rehner, M. Sterns, D. Schneiderbanger, S. Martius, and L. P. Schmidt, "A quasi-lumped ultra-broadband contiguous SSL-diplexer from DC to 80 GHz," in *2009 IEEE MTT-S International Microwave Symposium Digest*, pp. 1037–1040, Boston, MA, USA, 2009.

[17] I. Ashiq and A. P. Khanna, "Ultra-broadband contiguous planar DC-35-65 GHz diplexer using softboard suspended stripline technology," in *2013 IEEE MTT-S International Microwave Symposium Digest (MTT)*, pp. 1–4, Seattle, WA, USA, 2013.

[18] I. Ashiq and A. Khanna, "A novel ultra-broadband DC-36-to-66-GHz hybrid diplexer using waveguide and SSL technology," in *2014 44th European Microwave Conference*, pp. 1111–1114, Rome, Italy, 2014.

[19] I. Ashiq and A. P. Khanna, "A novel planar contiguous diplexer DC-67-100 GHz using organic liquid crystal polymer (LCP)," in *2015 IEEE MTT-S International Microwave Symposium*, pp. 1–4, Phoenix, AZ, USA, 2015.

[20] R. M. Dougherty, "MM-wave filter design with suspended stripline," *Microwave Journal*, vol. 29, p. 75, 1986.

[21] S. A. Alseyab, "A novel class of generalized Chebyshev lowpass prototype for suspended substrate stripline filters," *IEEE Transactions on Microwave Theory and Techniques*, vol. 30, no. 9, pp. 1341–1347, 1982.

[22] P. Bhartia and P. Pramanick, "Computer-aided design models for broadside-coupled striplines and millimeter-wave suspended substrate microstrip lines," *IEEE Transactions on Microwave Theory and Techniques*, vol. 36, no. 11, pp. 1476–1481, 1988.

[23] G. L. Mathaei, L. Young, and E. M. T. Jones, *Microwave Filters, Impedance-Matching Networks, and Coupling Structures*, Artech House, Harwood, MA, 1980.

[24] S. B. Cohn, "Characteristic impedances of broadside-coupled strip transmission lines," *IEEE Transactions on Microwave Theory and Techniques*, vol. 8, no. 6, pp. 633–637, 1960.

[25] R. Sturvidant, "A capacitively coupled BPF design using a suspended substrate stripline," *Microwave Journal*, vol. 36, pp. 71–74, 1993.